Neural Networks 23 (2010) 698–704

Contents lists available at ScienceDirect

Neural Networks

journal homepage: www.elsevier.com/locate/neunet

2010 Special Issue

Estimation of genuine and random synchronization in multivariate neural series

Dong Cui [a,d], Xianzeng Liu [b], You Wan [c], Xiaoli Li [d,*]

[a] Institute of Information Science and Engineering, Yanshan University, Qinhuangdao 066004, China

[b] The Comprehensive Epilepsy Center, Departments of Neurology and Neurosurgery, Peking University People's Hospital, No. 11 Xi Zhi Men Wai South Street, Xi Cheng District, Beijing 100044, China

[c] Neuroscience Research Institute, Peking University and Key Lab for Neuroscience, Ministry of Education, 38 Xueyuan Road, Beijing 100191, China

[d] Institute of Electrical Engineering, Yanshan University, Qinhuangdao 066004, China

ARTICLE INFO

Article history:
Received 1 October 2009
Received in revised form 25 March 2010
Accepted 18 April 2010

Keywords:
Genuine synchronization
Random synchronization
Multivariate neural series
Multi-channel neural mass model
Epilepsy

ABSTRACT

Synchronization is an important mechanism that helps in understanding information processing in a normal or abnormal brain. In this paper, we propose a new method to estimate the genuine and random synchronization indexes in multivariate neural series, denoted as GSI (genuine synchronization index) and RSI (random synchronization index), by means of a correlation matrix analysis and surrogate technique. The performance of the method is evaluated by using a multi-channel neural mass model (MNMM), including the effects of different coupling coefficients, signal to noise ratios (SNRs) and time-window widths on the estimation of the GSI and RSI. Results show that the GSI and the RSI are superior in description of the synchronization in multivariate neural series compared to the S-estimator. Furthermore, the proposed method is applied to analyze a 21-channel scalp electroencephalographic recording of a 35 year-old male who suffers from mesial temporal lobe epilepsy. The GSI and the RSI at different frequency bands during the epileptic seizure are estimated. The present results could be helpful for us to understand the synchronization mechanism of epileptic seizures.

1. Introduction

In neurological studies, synchronization is recognized as a key feature to indicate the information process in a normal or abnormal brain (e.g. Buzsáki, 2004; Buzsáki & Draguhn, 2004; Fell et al., 2001; Varela, Lachaux, Rodriguez, & Martinerie, 2001). The estimated synchronization of the experimental and clinical data, for instance multivariate neural signals, become the signatures of brain pathologies, or brain functions, or the early diagnosis and monitoring of brain disorder. (Aarabi, Wallois, & Grebe, 2008; Carmeli, Knyazeva, Innocenti, & De Feo, 2005; Darvas, Ojemann, & Sorensen, 2009; Knyazeva et al., 2008; Rudrauf et al., 2005; Stam, Jones, Nolte, Breakspear, & Scheltens, 2007). In order to investigate synchronization in the brain, multiple electrodes are often used to record the neural signals in different areas of the brain simultaneously. Therefore, how to estimate the synchronization index of multivariate neural signals has become a crucial issue in neural signal processing.

Some methods have been developed to estimate the synchronization index (or correlation coefficient) between two neural series, for instance cross-correlation, spectrum-based coherence, synchronization likelihood, mutual information, nonlinear interdependence, phase synchronization, correntropy coefficient, event synchronization, and so on (Arnhold, Lehnertz, Grassberger, & Elger, 1999; Brown & Kocarev, 2000; Bruns, 2004; Carter, 1987; Lachaux, Rodriguez, Martinerie, & Varela, 1999; Le Van Quyen et al., 2005; Quian Quiroga, Kraskov, Kreuz, & Grassberger, 2002; Quian Quiroga, Kreuz, & Grassberger, 2002; Stam & van Dijk, 2002; Xu, Bakardjian, Cichocki, & Principe, 2008). To analyze multivariate neural series, we may repetitively use bivariate measure methods to obtain the synchronization index among neural series. However, how to obtain a golden synchronization index in multivariate neural signals is still a bottleneck problem (Allefeld & Kurths, 2004; Pereda, Quian Quiroga, & Bhattacharya, 2005). Recently, an S-estimator has been developed to estimate the synchronization in multi-channel EEG series (Carmeli et al., 2005). In this method, the quantified synchronization is inversely proportional to the embedding dimension of the dynamical system, and is independent of the total power and the time dimension of the neural signals. The disadvantage of the S-estimator is that the estimated synchronization index includes random and/or artifact components, because the synchronization is often estimated over finite-length data, so the estimated synchronization includes, to some extent, random and/or artifact information (Müller, Baier, Rummel, & Schindler, 2008; Plerou et al., 2002). In a recent study, a concept of genuine synchronization was proposed for the first time by

* Corresponding author.
E-mail address: xiaoli.avh@gmail.com (X. Li).

0893-6080/$ – see front matter © 2010 Elsevier Ltd. All rights reserved.
doi:10.1016/j.neunet.2010.04.003

Müller et al. (2008) to remove the random (and/or artifact) components in multivariate neural signals. In this method, the genuine cross-correlation strength (TCS) was estimated by means of the significant deviation of the eigenvalues (or partial eigenvalues) of the linear zero-lag cross-correlation matrix. However, all of eigenvalues contain rich information (Kwapień, Drożdż, & Oświeçimka, 2006), so this information should be used.

In this paper, we propose a method to estimate the GSI and the RSI in multivariate neural signals. To test the performance of the method, a multi-channel neural mass model (MNMM) (Cui, Li, & Gu, 2009) is applied to generate multivariate neural signals. The effects of different coupling coefficients, signal to noise ratios (SNRs) and time-window widths on the method are investigated. Application of the method to the multivariate long-term EEG recording of a 35 year-old male suffering from mesial temporal lobe epilepsy is demonstrated as well.

2. Methods

2.1. Correlation matrix analysis

Equal-time correlation is a simple method to measure the synchronization between two series. Consider multivariate neuronal data $\mathbf{Z} = \{z_i(n)\}$, $i = 1, \ldots, M$, $n = 1, \ldots, T$, where M is the channel number and n is the number of data points in time window T. To provide the same scale for all the neuronal population activities, the normalized data $\mathbf{X} = \{x_i(n)\}$ are first calculated by $x_i(n) = (z_i(n) - \langle Z_i \rangle)/\sigma_i$, where $\langle Z_i \rangle$ and σ_i are the mean and standard deviation of $z_i(n)$, respectively. Then the equal-time correlation matrix can be constructed as

$$\mathbf{C} = \frac{1}{T} XX', \tag{1}$$

where the superscript denotes transposition. It is noted that we can also select other correlation methods to construct the correlation matrix $\mathbf{C}$, such as phase synchronization, synchronization likelihood, mutual information, nonlinear interdependency and event synchronization. The selection of the method depends on the nature of the data being analyzed.

The eigenvalue decomposition of $\mathbf{C}$ is

$$\mathbf{C}\mathbf{v}_i = \lambda_i \mathbf{v}_i, \tag{2}$$

where eigenvalues $\lambda_1 \leq \lambda_2 \leq \cdots \leq \lambda_M$ are in increasing order and $v_i, i = 1, \ldots, M$ are the corresponding eigenvectors. As $\mathbf{C}$ is a real symmetric matrix, all eigenvalues are real numbers, and the trace of $\mathbf{C}$ is equal to the number of series M. When all the time series are correlated perfectly, the entries of matrix $\mathbf{C}$ are all equal to 1. The maximum eigenvalue is M and the others are zeros. However, in practice, even though all the time series are uncorrelated completely, the computed correlation coefficients are not zeros due to the effect of the length of the data, and they follow a bell-shaped distribution (i.e. they are random correlations or artifact information). More universal properties of random matrices can be found in (Allefeld, Müller, & Kurths, 2007; Müller & Baier, 2005; Plerou et al., 2002; Seba, 2003; Wilcox & Gebbie, 2007).

2.2. Surrogate

When the multivariate time series are derived from an independent linear stochastic process, the ideal correlations between time series are zeros. Unfortunately, due to the effect of the algorithm and the length of the data, the calculated correlations exhibit a little bias, and are not purely zero. In this paper, a surrogate method is used to reduce the 'bias' (i.e. random correlations or artifact information) in practical time series. The surrogate method proposed by Andrzejak, Kraskov, Stögbauer, Mormann, and Kreuz (2003) is employed, which iteratively permutes the original sample values of each series. Details can be found in the Appendix. The randomized multivariate data have the same size (channel number M and the number of data points n in time window T) and in particular the same power spectrum of each time series as its original time series. Based on the surrogate series, the equal-time surrogate correlation matrix $\mathbf{R}$ can be calculated: $\lambda_1^s \leq \lambda_2^s \leq \cdots \leq \lambda_M^s$ are denoted as the eigenvalues of surrogate matrix $\mathbf{R}$. The distribution of the surrogate eigenvalues λ_i^s can reflect the random synchronization of the multivariate time series.

2.3. GSI and RSI estimator

The S-estimator has been proposed to assess synchronization in multivariate EEG series by means of the distributions of the eigenvalues of the covariance matrix (Carmeli et al., 2005). The normalized eigenvalues $\lambda_i^{(1)}$ of the covariance matrix are defined as follows:

$$\lambda_i^{(1)} = \frac{\lambda_i}{\sum_{i=1}^{M} \lambda_i}, \quad i = 1, \ldots, M. \tag{3}$$

For a random multivariate time series, the minimum and maximum eigenvalues of the random correlation matrix are $\lambda_{\min,\max} = 1 + \frac{1}{Q} \pm 2\sqrt{\frac{1}{Q}}$, $Q = T/M$. That is to say, although all the multivariate time series are not correlated, the eigenvalues range in the bound $[\lambda_{\min}, \lambda_{\max}]$ (Plerou et al., 2002; Seba, 2003). The calculated S-estimator is a non-zero value for random multiviate time series (Müller et al., 2008; Plerou et al., 2002). The S-estimator (total synchronization) is composed of genuine and random synchronizations. To reduce the effects of the random components in the total synchronization, the eigenvalues are divided by the averaged surrogate eigenvalues; that is,

$$\lambda_i^{(2)} = \frac{\lambda_i / \bar{\lambda}_i^s}{\sum_{i=1}^{M} \lambda_i / \bar{\lambda}_i^s}, \quad i = 1, \ldots, M, \tag{4}$$

where $\bar{\lambda}_i^s$ is the average eigenvalues of the surrogate series over the SN realizations.

In a similar manner, the normalized surrogate eigenvalues are obtained as follows:

$$\lambda_i^{(3)} = \frac{\bar{\lambda}_i^s}{\sum_{i=1}^{M} \bar{\lambda}_i^s}, \quad i = 1, \ldots, M. \tag{5}$$

All the synchronization indexes can be summarized as follows:

$$SI^{(k)} = 1 + \frac{\sum_{i=1}^{M} \lambda_i^{(k)} \log\left(\lambda_i^{(k)}\right)}{\log(M)}, \quad k = 1, 2, 3. \tag{6}$$

When $k = 1$ (Eq. (3)), this is an S-estimator, which is a measure of the total amount of synchronization (Carmeli et al., 2005); when $k = 2$ (Eq. (4)), the eigenvalues of $\lambda_i^{(2)}$ are applied, and the genuine synchronization index (GSI) is obtained. To understand how this measure works, two cases should be considered. If genuine correlation does not exist, the normalized eigenvalues $\lambda_i^{(2)}$ are all equal to $1/M$, so $SI^{(2)} = 0$; on the other hand, if all the time series are correlated perfectly, the largest eigenvalue $\lambda_M = M$, and the others are equal to zero, i.e. the largest normalized eigenvalue is $\lambda_M^{(2)} = 1$, and the others are zero, so $SI^{(2)} = 1$. The random synchronization index (RSI) can be obtained when $k = 3$ (Eq. (5)).

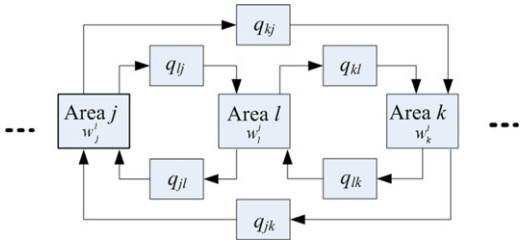

Fig. 1. Schematic diagram of the multi-channel neural mass model. The coupling coefficient q_{jk} means the coupling from area j to area k. The weighting parameters w_j^i, $i = 1, 2, \ldots, N$ adjust the multi-kinetics of the multi-channel neural mass model.

2.4. MNMM for simulation

A neural mass model (NMM) can generate simulated data that are very similar to real EEG signals (David, Cosmelli, & Friston, 2004; Ursino, Zavaglia, Astolfi, & Babiloni, 2007; Wendling, Bellanger, Bartolomei, & Chauvel, 2000; Zavaglia, Astolfi, Babiloni, & Ursino, 2008). In this study, a modified multi-channel neural mass model (MNMM) proposed by Cui et al. (2009) is used to test whether the GSI and the RSI are able to track the amount of genuine synchronization and random synchronization in multivariate neural data. The MNMM can simulate the massive interactions in neuronal populations with excitatory couplings among remote cortical areas, and generate similar neural signals. The performance of these measures can be demonstrated with the MNMM.

Fig. 1 plots a simple schematic description of the MNMM. In each area, a multi-kinetics neural mass model is built to generate a channel of EEG signals (David & Friston, 2003). For a given area j, the model is composed of N subpopulations (or N linear transfer functions) in parallel. Each subpopulation has different kinetics. The relative size of each subpopulation is determined by the weight coefficient w_j^i, $i = 1, \ldots, N$, where $w_j^i \in [0, 1]$ and $\sum_{i=1}^{N} w_j^i = 1$. The spectrum of simulated EEG signals is adjusted by the coupling weight coefficients. q_{jk} $(j, k = 1, \ldots, M)$ denotes the coupling coefficient from area j to channel k.

The differential equations that govern the MNMM are as follows:

$$\begin{cases} \dot{y}_0^{ji} = y_3^{ji} \\ \dot{y}_1^{ji} = y_4^{ji} \\ \dot{y}_2^{ji} = y_5^{ji} \\ \dot{y}_3^{ji} = \dfrac{H_e^i}{\tau_e^i} \cdot S\left(\sum_{i=1}^{N} w_j^i y_1^{ji} - \sum_{i=1}^{N} w_j^i y_2^{ji}\right) - \dfrac{2y_3^{ji}}{\tau_e^i} - \dfrac{y_0^{ji}}{\left(\tau_e^i\right)^2} \\ \dot{y}_4^{ji} = \dfrac{H_e^i}{\tau_e^i} \cdot \left[p_j(t) + C_2 S\left(C_1 \sum_{i=1}^{N} w_j^i y_0^{ji}\right) \right. \\ \qquad \left. + RM\left(\sum_{k=1,k\neq j}^{M} q_{jk} S\left(\sum_{i=1}^{N} w_k^i y_{1\_\tau}^{ji} - \sum_{i=1}^{N} w_k^i y_{2\_\tau}^{ji}\right)\right)\right] \\ \qquad - \dfrac{2y_4^{ji}}{\tau_e^i} - \dfrac{y_1^{ji}}{\left(\tau_e^i\right)^2} \\ \dot{y}_5^{ji} = \dfrac{H_i^i}{\tau_i^i} \cdot C_4 S\left(C_2 \sum_{i=1}^{N} w_j^i y_0^{ji}\right) - \dfrac{2y_5^{ji}}{\tau_i^i} - \dfrac{y_2^{ji}}{\left(\tau_i^i\right)^2}. \end{cases} \tag{7}$$

The simulated EEG signals of channel j are

$$EEG_j = \sum_{i=1}^{N} w_k^i y_{1\_\tau}^{ji} - \sum_{i=1}^{N} w_k^i y_{2\_\tau}^{ji}, \tag{8}$$

where $j = 1, 2, \ldots, M$ is the channel number; $i = 1, 2, \ldots, N$ are N parallel subpopulations with different kinetics; $H_e(H_i)$ is the average excitatory (or inhibitory) synaptic gain and $\tau_e(\tau_i)$ is a lumped representation of the sum of the rate constants of the passive membrane and other spatially distributed delays in the dendritic tree. A nonlinear function $S(v) = 2e_0/(1 + e^{r(v_0 - v)})$ transforms the average membrane potential of the population into an average rate of action potentials fired by the neuronal networks. The connectivity constants C_1, C_2, C_3, C_4 are the average numbers of synaptic connections between the pyramidal cells and the interneurons. The input of area j is a mixture of a Gaussian noise $p_j(t)$, which contains inputs from the other uncertain areas; the excitatory feedback from pyramidal cells is $C_2 S\left(C_1 \sum_{i=1}^{N} w_j^i y_0^{ji}\right)$ and the coupling signal from the other areas is $RM\left(\sum_{k=1,k\neq j}^{M} q_{jk} S\left(\sum_{i=1}^{N} w_k^i y_{1\_\tau}^{ji} - \sum_{i=1}^{N} w_k^i y_{2\_\tau}^{ji}\right)\right)$. The coupling signals are delayed with a propagation time, τ, which is indicated by the subscript in $y_{1\_\tau}^{ji}$ and $y_{2\_\tau}^{ji}$. To keep the equilibrium of each population, a function $RM(x) = x - mean(x)$ is used to remove the mean value of the coupling signals.

In this study, the channel number of the simulated EEG time series is set as $M = 10$. Each area has the same dynamics, composed of $N = 3$ parallel subpopulations. Each subpopulation can generate delta, alpha and gamma rhythms by adjusting the $\mathbf{W} = [w_j^1, w_j^2, w_j^3], j = 1, \ldots, M$. The coupling coefficients are $q_{jk} = q\ (j, k = 1, \ldots, M, j \neq k)$ for all areas. The extrinsic inputs $p_j(t)$ have the same mean value $\langle p_j \rangle = 220$ and standard deviation $\sigma_{p_j} = 22$. The propagation time delay τ is set as 10 ms. The sampling frequency is 500 Hz. Other specified parameters in the MNMM can be found in (Cui et al., 2009; David & Friston, 2003).

2.5. Real EEG data

A long-term EEG recording from a 35 year-old male patient who suffers from mesial temporal lobe epilepsy is employed to test the method proposed in this study. The data was collected from 21 scalp electrodes placed according to the international 10–20 System with additional electrodes T1 and T2 on the temporal region. The sampling frequency was 250 Hz and an average reference was applied. The free datasets can be found and downloaded at the website http://www.cs.tut.fi/~gomezher/projects/eeg/databases.htm. The details of the datasets have been addressed in (De Clercq, Vergult, Vanrumste, Van Paesschen, & Van Huffel, 2006; Vergult et al., 2007).

3. Results

3.1. Simulation analysis

3.1.1. Simulated multivariate EEG series

Typical simulated EEG series of the 10 channels and corresponding normalized spectra of different coupling coefficients are shown in Fig. 2. The weight parameter is $\mathbf{W} = [0.4, 0.3, 0.3]$. With the increase of coupling strength, the spectra of simulated EEG series vary from multiple frequencies to a single and low frequency.

3.1.2. The effects of frequency band on the S-estimator, the GSI and the RSI

The uncoupled EEG series are simulated by the MNMM with three different weight parameters. Fig. 3(a) shows the simulated 10-channel EEG series over 1 s. Fig. 3(b) shows the corresponding normalized spectra of one channel. The equal-time correlation matrices are plotted in Fig. 3(c): the different gray levels (colors) represent different cross-correlations between two channels series. Fig. 3(d) shows the mean and standard deviations of the S-estimator, the GSI and the RSI of three different signals

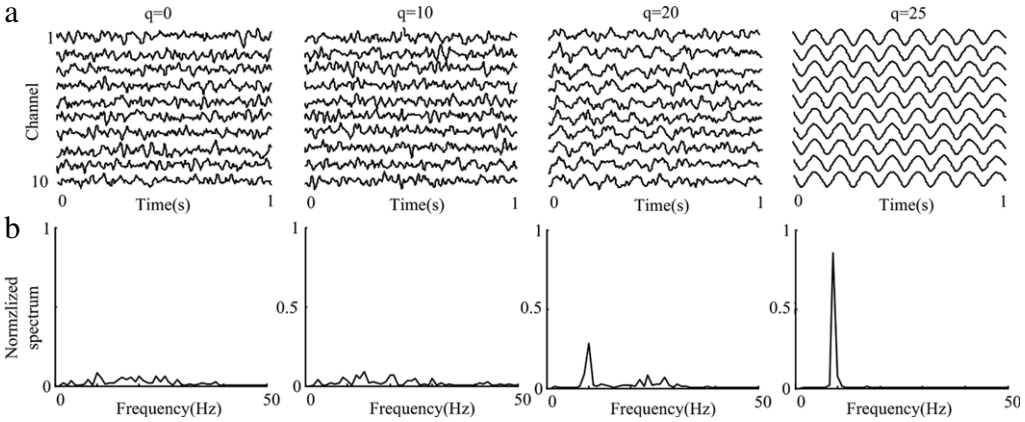

Fig. 2. The simulated EEG series and their spectra. (a) Simulated EEG series of the 10 channels with a multi-channel neural mass model. The simulated EEG series are generated with four different coupling coefficients ($q_{jk} = q = [0, 10, 20, 25]$, $j, k = 1, \ldots, 10$, $j \neq k$); and the weight coefficient of each area is the same ($\mathbf{W} = [0.4, 0.3, 0.3]$). (b) The corresponding normalized spectra of the simulated EEG series.

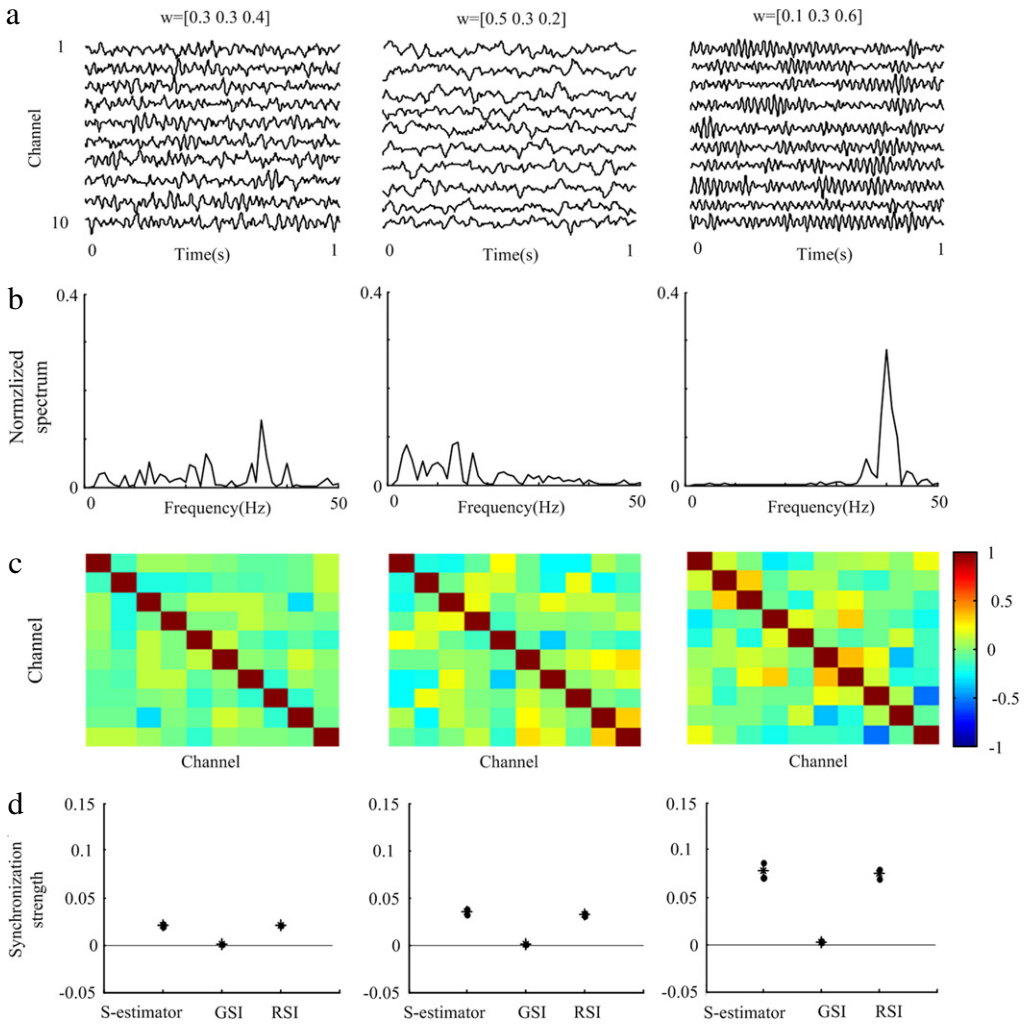

Fig. 3. The S-estimator, the GSI and the RSI of the uncoupled EEG series. (a) The 10-channel EEG series without coupling generated by the MNMM with three different weight coefficients ($\mathbf{W} = [0.3, 0.3, 0.4]$, $\mathbf{W} = [0.5, 0.3, 0.2]$ and $\mathbf{W} = [0.1, 0.3, 0.6]$). (b) The normalized spectra of an EEG series. (c) The equal-time correlation matrices constructed by cross-correlation. (d) The mean values and standard deviations of the S-estimator, the GSI and the RSI.

over 50 realizations. In this study, the averages of eigenvalues $\bar{\lambda}_i^s$ of surrogated series are computed over $SN = 100$ realizations for each interval.

In the left column ($\mathbf{W} = [0.3, 0.3, 0.4]$), the spectrum bandwidth of the simulated series is broad. The elements of the correlation matrices are not equal to zeros, namely a random correlation is involved; the bias is derived from the correlation computation that is based on a finite series. As shown in Fig. 3(d), the S-estimator and the RSI are greater than zero; however, the GSI tends to zero. In the middle column, the main frequencies

of simulated signals vary from high frequency to low frequency due to the change of relative size of the three subpopulations ($\mathbf{W} = [0.5, 0.3, 0.2]$). The correlation matrix increases a little, which results in an increase of the S-estimator and the RSI, but the GSI still tends to zero. In the right column ($\mathbf{W} = [0.1, 0.3, 0.6]$), the frequency band of the simulated signals is narrow and a gamma rhythm can be seen. The correlation matrix is more significant, and the S-estimator and the RSI both increase, too. However, the GSI is still close to zero. Therefore, the change of frequency band cannot result in a big change on the genuine correlation strength. It is obvious that the GSI is insensitive to this change; thus the GSI is better in indicating the synchronization of the multi-channel EEG series than the S-estimator.

3.1.3. The effect of the coupling strength, the SNR and the time-window width

To evaluate the effect of the coupling coefficients, the SNRs and the time-window widths to the S-estimator, the GSI and the RSI, the simulated EEG series of MNMM are analyzed and shown in Fig. 4. Fig. 4(a) plots the mean and standard deviations (over 50 realizations) of the three synchronization indexes as a function of the coupling coefficient q: q ranges from 10 to 25 with a step of 1. The length of the time window for the data analyzed is 1 s. In Fig. 4(a), when the coupling coefficient ranges from 10 to 14 (i.e. weak couplings), the mean of the S-estimator is 0.0204, 0.0210, 0.0239, 0.0244 and 0.0234, respectively. The mean of RSI is 0.0210, 0.0212, 0.0215, 0.0218, 0.0214 and the mean of the GSI is 0.0006, 0.0008, 0.0008, 0.0011, 0.0008. The S-estimator and the RSI are greater than zero, but the GSI is close to zero. Therefore, the GSI does not contain random and artifact synchronization. This result is similar to that in Fig. 3. With the increase of the coupling strength, all of the three synchronization indexes increase. When the coupling strength, q, is greater than 23, the S-estimator is close to 1; however the GSI is less than 1, because the effect of the random component on the GSI is slight. These results demonstrate that the GSI can reveal a true synchronization in multivariate neural series.

Fig. 4(b) shows the effects of noise on the S-estimator, the GSI and the RSI. The three synchronization indexes over different SNRs are analyzed. The length of the time window is 1 s and the coupling coefficient q is set as 20. By adding white noise with different SNR (0–40 dB), it can be seen that the white noise of different SNR has a significant effect on these measures. When the noise is heavy, the three synchronization indexes are smaller than the real values. With the increase of the SNR, these measures tend to the real synchronization values.

The S-estimator, the GSI and the RSI as a function of the window width are analyzed and the result is shown in Fig. 4(c). The coupling coefficient q is set as 20. The length of the time window varies from 0.5 to 4 s with a step of 0.5 s. With the increase of the window width, the RSI decreases. It is obvious that the random synchronization decreases with the increase of the length of the data. The S-estimator does not change over different time-window widths. However, the GSI increases a little because the effect of random correlations is reduced with the increase of the time-window width. Thus, the GSI is superior in revealing the true synchronization value compared with the S-estimator.

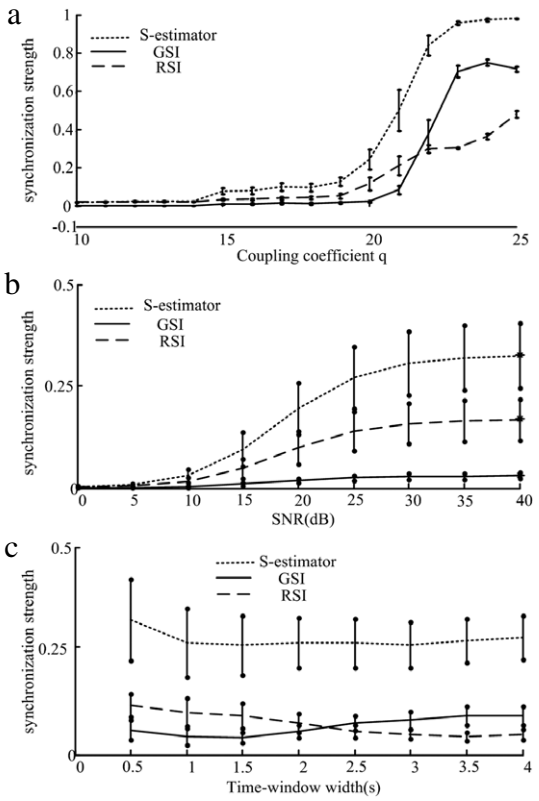

Fig. 4. The S-estimator (dotted lines), the GSI (solid lines) and the RSI (dashed lines) of the simulated EEG series generated by the MNMM. (a) The effect of the coupling coefficients on the S-estimator, the GSI and the RSI. (b) The effect of the SNR on the S-estimator, the GSI and the RSI. (c) The effect of the time-window width on the S-estimator, the GSI and the RSI.

3.2. Analysis of epileptic scalp EEG data

Fig. 5 shows the raw 21-channel EEG data and the S-estimator, the GSI and the RSI over time. Consider the propagation mechanism of a partial seizure (the delay between two EEG series at different channels): the correlation matrix should be constructed by means of a phase synchronization method. The phase of the time series is extracted by a Morlet wavelet transform (Quian Quiroga, & Kraskov et al., 2002; Quian Quiroga, & Kreuz et al., 2002). Fig. 5(a) plots the 21-channel EEG recordings over 300 s, including a full ictal event. A moving window technique (window of 10 s with an overlap of 5 s) is applied; the three synchronization indexes at the different frequency bands are computed and shown in Fig. 5(b–d). The S-estimator, the GSI and the RSI of the EEG data for the frequency bands 1–12 Hz, 12–30 Hz and 30–80 Hz are plotted, respectively. In Fig. 5(b) and (c), the S-estimator and the GSI have a significant increase for the duration of the ictal state. In Fig. 5(b), due to the effect of random synchronization at the beginning of the ictal state, the S-estimator is more significant, but it is not a real synchronization. At the frequency band 12–30 Hz (Fig. 5(c)), the S-estimator is significant, similar to the GSI, and the random synchronization at the ictal state is significant. In Fig. 5(d), during the interictal period the RSI for the frequency band 30–80 Hz is significant; however it is very weak for the duration of ictal state, and thus the S-estimator cannot find a real synchronization to indicate an ictal event. In contrast, the GSI can still track the ictal event for the frequency band 30–80 Hz because of the removal of the random component. In short, the GSI is superior to the S-estimator in estimating the synchronization in multi-channel EEG recordings.

4. Conclusions

In this paper, the GSI and the RSI are proposed to quantify a genuine synchronization and a random synchronization in multivariate neural series by means of a correlation matrix analysis and the surrogate method. A multi-channel neural mass model is employed to generate multi-channel neural time series; then the performance of the proposed method is evaluated by the simulated

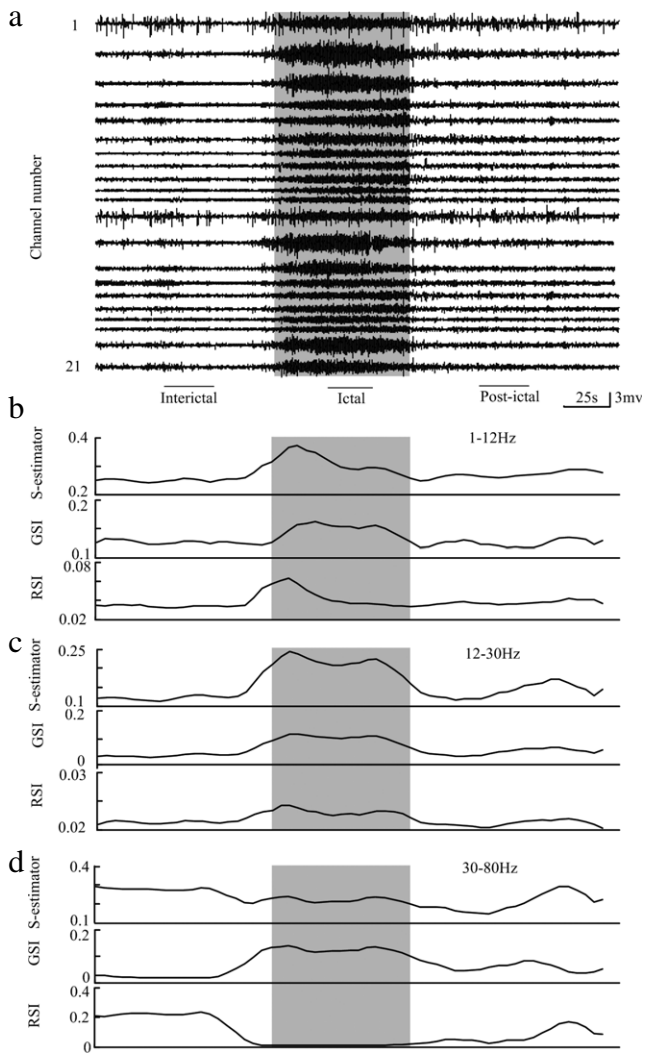

Fig. 5. The S-estimator, the GSI and the RSI for multi-channel epileptic scalp EEG recordings. (a) The raw EEG recording from interictal to post-ictal state over 300 s. The shadow region denotes the ictal stage of the epileptic seizure. (b) The S-estimator, the GSI and the RSI over time for the frequency band 1–12 Hz; (c) The S-estimator, the GSI and the RSI over time for the frequency band 12–30 Hz; (d) The S-estimator, the GSI and the RSI over time for the frequency band 30–80 Hz.

EEG series, including the effect of the frequency of EEG signals, coupling coefficients, SNRs and time-window widths. Finally, the method is applied to analyze a 21-channel scalp EEG recording of a patient suffering from mesial temporal lobe epilepsy. Based on the findings and results, the following conclusions can be made.

(1) The proposed GSI and RSI can be applied to indicate genuine and random synchronization in multivariate EEG series at different frequency bands; in particular, the GSI is insensitive to the frequency bands.
(2) The proposed GSI is more robust to the coupling strength and widow width than the S-estimator.
(3) The GSI is better at indicating the synchronization of epileptic EEG signals at different frequency bands than the S-estimator.

Several methods have been developed to estimate the synchronizations of multivariate neural signals, including phase synchronization cluster analysis (Allefeld & Kurths, 2004), graph theoretic analysis (Stam et al., 2007), frequency flows and time–frequency dynamics analysis (Rudrauf et al., 2005) and the mixture-of-Gaussians analysis (Matsumoto, Okada, Sugase-Miyamoto, Yamane, & Kawano, 2005). These methods can identify the structure of statistical phase synchronization clusters, or give the characteristic of network connection, or track and characterize the non-stationary time–frequency dynamics of phase synchrony among groups or assemblies directly, or reveal the number of clusters and the elements of each channel, respectively. However, these methods cannot directly quantify the global synchronization in multivariate neural signals. Recently, other methods, such as the S-estimator (Carmeli et al., 2005), multivariate phase synchronization (Boccaletti, Kurths, Osipov, Valladares, & Zhou, 2002; Knyazeva et al., 2008) and correlation matrix analysis (CMA) (Li et al., 2007), have been developed to quantify the global synchronization. In this study, we concentrate on the decomposition of the genuine and random synchronization in multivariate neural signals. The idea for this method follows the one proposed by Müller et al. (2008). In the method proposed by Müller et al. (2008), the total, genuine and random cross-correlation strengths (TCS, CCS and RCS) can be estimated. However, these indexes are only based on the maximal and minimal eigenvalues. In the method proposed in this paper, all the eigenvalues are used; this is the main difference between our method and the method proposed by Müller et al. (2008).

Acknowledgements

This work was supported by Program for New Century Excellent Talents in University (NECT-07-0735), National Natural Science Foundation of China (90820016), Natural Science Foundation of Hebei and "973" Program of China (2007CB512501).

Appendix

In this study, a bivariate surrogate technique proposed by (Andrzejak et al., 2003) is applied. In this surrogate method, all the nonlinear interdependences are destroyed by a randomization scheme and the self-linear properties of time series are retained. A random shuffle of the original sample values $x_i(n)$, $n = 1, \ldots, T$, $\tilde{x}_i(n)$ is generated which is used as a seed for the iteration scheme. The surrogate procedure is as follows. First, the Fourier transform of seed $\tilde{x}_i(n)$ is calculated and the Fourier spectrum $\left\{\tilde{a}_i(k)\, e^{j\tilde{\varphi}_{ik}}\right\}^{(p)}$ is obtained; the amplitudes $\tilde{a}_i(k)$ are replaced with the original amplitudes $a_i(k)$ of $x_i(n)$, but the randomized phases $\tilde{\varphi}_{ik}$ are remained. Second, the smallest, second smallest, . . ., highest values of $\tilde{x}_i(n)^{(p)}$ are replaced by the smallest, second smallest, . . ., highest value of $x_i(n)$, so a new seed $\tilde{x}_i(n)^{(p+1)}$ can be generated to start a new iteration step. Repeating the above steps many times, a surrogate realization $\tilde{x}_i(n)^{(p+1)}$ is obtained and the amplitudes $\left\{\tilde{a}_i(k)\right\}^{(p)}$ converge to $a_i(k)$.

References

Aarabi, A., Wallois, F., & Grebe, R. (2008). Does spatiotemporal synchronization of EEG change prior to absence seizures?. *Brain Research*, *1188*, 207–221.
Allefeld, C., & Kurths, J. (2004). An approach to multivariate phase synchronization analysis and its application to event-related potentials. *International Journal of Bifurcation and Chaos*, *14*(2), 417–426.
Allefeld, C., Müller, M., & Kurths, J. (2007). Eigenvalue decomposition as a generalized synchronization cluster analysis. *International Journal of Bifurcation and Chaos*, *17*(10), 3493–3497.
Andrzejak, R. G., Kraskov, A., Stögbauer, H., Mormann, F., & Kreuz, T. (2003). Bivariate surrogate techniques: necessity, strengths, and caveats. *Physics Review E*, *68*, 066202.
Arnhold, J., Lehnertz, K., Grassberger, P., & Elger, C. E. (1999). A robust method for detecting interdependences: application to intracranially recorded EEG. *Physica D*, 134–419.
Boccaletti, S., Kurths, J., Osipov, G., Valladares, D. L., & Zhou, C. S. (2002). The synchronization of chaotic systems. *Physics Reports*, *366*(1), 1–101.
Brown, R., & Kocarev, L. (2000). A unifying definition of synchronization for dynamical systems. *Chaos*, *10*(2), 344–349.

Bruns, A. (2004). Fourier-, Hilbert- and wavelet-based signal analysis: are they really different approaches?. *Journal of Neuroscience Methods*, *137*, 321–332.
Buzsáki, G. (2004). Large-scale recording of neuronal ensembles. *Nature Neuroscience*, *7*, 446–451.
Buzsáki, G., & Draguhn, A. (2004). Neuronal oscillations in cortical networks. *Science*, *304*, 1926–1929.
Carmeli, C., Knyazeva, M. G., Innocenti, G. M., & De Feo, O. (2005). Assessment of EEG synchronization based on state-space analysis. *NeuroImage*, *25*, 339–354.
Carter, G. C. (1987). Coherence and time delay estimation. *Proceedings of IEEE*, *75*(12), 236–255.
Cui, D., Li, X. L., & Gu, G. H. (2009). *Neural Mass Modeling for Multi-channel EEG Synchronization Analyzing*. Paper presented at the meeting of the 2nd International Conference on BioMedical Engineering and Informatics, Tianjin, (pp. 291–295).
Darvas, F., Ojemann, J. G., & Sorensen, L. B. (2009). Bi-phase locking—a tool for probing non-linear interaction in the human brain. *NeuroImage*, *46*, 123–132.
David, O., Cosmelli, D., & Friston, K. J. (2004). Evaluation of different measures of functional connectivity using a neural mass model. *NeuroImage*, *21*, 659–673.
David, O., & Friston, K. J. (2003). A neural mass model for MEG/EEG: coupling and neuronal dynamics. *NeuroImage*, *20*, 1743–1755.
De Clercq, W., Vergult, A., Vanrumste, B., Van Paesschen, W., & Van Huffel, S. (2006). Canonical correlation analysis applied to remove muscle artifacts from the electroencephalogram. *IEEE Transactions on Biomedical Engineering*, *53*, 2583–2587.
Fell, J., Klaver, P., Lehnertz, K., Grunwald, T., Schaller, C., Elger, C. E., et al. (2001). Human memory formation is accompanied by rhinal-hippocampal coupling and decoupling. *Nature Neuroscience*, *4*, 1259–1264.
Knyazeva, M. G., Jalili, M., Brioschi, A., Bourquin, I., Fornari, E., Hasler, M., et al. (2008). Topography of EEG multivariate phase synchronization in early Alzheimer's disease. *Neurobiology of Aging*, doi:10.1016/j.neurobiolaging.2008.07.019.
Kwapien, J., Drozdz, S., & Oswiecimka, P. (2006). The bulk of the stock market correlation matrix is not pure noise. *Physica A*, *359*, 589–606.
Lachaux, J., Rodriguez, E., Martinerie, J., & Varela, F. (1999). Measuring phase synchrony in brain signals. *Human Brain Mapping*, *8*, 194–208.
Le Van Quyen, M., Soss, J., Navarro, V., Robertson, R., Chavez, M., Baulac, M., et al. (2005). Preictal state identification by synchronization changes in longterm intracranial EEG recordings. *Clinical Neurophysiology*, *116*, 559–568.
Li, X. L., Cui, D., Jiruska, P., Fox, J., Yao, X., & Jefferys, J. G. R. (2007). Synchronization measurement of multiple neuronal populations. *Journal of Neurophysiology*, *98*, 3341–3348.
Matsumoto, N., Okada, M., Sugase-Miyamoto, Y., Yamane, S., & Kawano, K. (2005). Population dynamics of face-responsive neurons in the inferior temporal cortex. *Cerebral Cortex*, *15*, 1103–1112.
Müller, M., & Baier, G. (2005). Detection and characterization of changes of the correlation structure in multivariate time series. *Physics Review E*, *71*, 046116.
Müller, M., Baier, G., Rummel, C., & Schindler, K. (2008). Estimating the strength of genuine and random correlations in non-stationary multivariate time series. *Europhysics Letters*, *84*, 10009.
Pereda, E., Quian Quiroga, R., & Bhattacharya, J. (2005). Nonlinear multivariate analysis of neurophysiological signals. *Progress in Neurobiology*, *77*(1–2), 1–37.
Plerou, V., Gopikrishnan, P., Rosenow, B., Nunes Amaral, L. A., Guhr, T., & Stanley, H. E. (2002). Random matrix approach to cross correlations in financial data. *Physics Review E*, *65*, 066126.
Quian Quiroga, R., Kraskov, A., Kreuz, T., & Grassberger, P. (2002). Performance of different synchronization measures in real data: a case study on electroencephalographic signals. *Physics Review E*, *65*, 041903.
Quian Quiroga, R., Kreuz, T., & Grassberger, P. (2002). Event synchronization: a simple and fast method to measure synchronicity and time delay patterns. *Physics Review E*, *66*, 041904.
Rudrauf, D., Douiri, A., Kovach, C., Lachaux, J. P., Cosmelli, D., Chavez, M., et al. (2005). Frequency flows and the time–frequency dynamics of multivariate phase synchronization in brain signals. *Neuroimage*, *31*, 209–227.
Seba, P. (2003). Random matrix analysis of human EEG data. *Physical Review Letters*, *91*(19), 198104.
Stam, C. J., Jones, B. F., Nolte, G., Breakspear, M., & Scheltens, P. (2007). Small-world networks and functional connectivity in Alzheimer's disease. *Cerebral Cortex*, *17*, 92–99.
Stam, C. J., & van Dijk, B. W. (2002). Synchronization likelihood: an unbiased measure of generalized synchronization in multivariate data sets. *Physica D*, *163*, 236–251.
Ursino, M., Zavaglia, M., Astolfi, L., & Babiloni, F. (2007). Use of a neural mass model for the analysis of effective connectivity among cortical regions based on high resolution EEG recordings. *Biological Cybernetics*, *96*, 351–365.
Varela, F. J., Lachaux, J. P., Rodriguez, E., & Martinerie, J. (2001). The brain web: phase synchronization and large-scale integration. *Nature Reviews Neuroscience*, *2*, 229–239.
Vergult, A., De Clercq, Q., Palmini, A., Vanrumste, B., Dupont, P., Van Huffel, S., et al. (2007). Improving the interpretation of Ictal Scalp EEG: BSS-CCA algorithm for muscle artifact removal. *Epilepsia*, *48*(5), 950–958.
Wendling, F., Bellanger, J. J., Bartolomei, F., & Chauvel, P. (2000). Relevance of nonlinear lumped-parameter models in the analysis of depth-EEG epileptic signals. *Biological Cybernetics*, *83*, 367–378.
Wilcox, D., & Gebbie, T. (2007). An analysis of cross-correlations in an emerging market. *Physica A*, *375*, 584–598.
Xu, J. W., Bakardjian, H., Cichocki, A., & Principe, J. C. (2008). A new nonlinear similarity measure for multichannel signals. *Neural Networks*, *21*, 222–231.
Zavaglia, M., Astolfi, L., Babiloni, F., & Ursino, M. (2008). The effect of connectivity on EEG rhythms, power spectral density and coherence among coupled neural populations: analysis with a neural mass model. *IEEE Transactions on Biomedical Engineering*, *55*(1), 69–77.